Materials Characterization 149 (2019) 218–225

Contents lists available at ScienceDirect

Materials Characterization

journal homepage: www.elsevier.com/locate/matchar

A transmission electron microscopy study of precipitate phases that form during operation in a heat exchanger alloy

Calin Daniel Marioara[a,*], Jesper Friis[a], Emmanuel Hersent[b], Anders Oskarsson[b]

[a] SINTEF Industry, 7465 Trondheim, Norway
[b] Gränges R&I, 612 81 Finspång, Sweden

ARTICLE INFO

Keywords:
Transmission electron microscopy (TEM)
Al-Mg-Si alloy
Precipitate crystal structure
Heat exchangers

ABSTRACT

During manufacturing of heat exchangers, the core material is cladded with a lower-melting point alloy, rolled into thin strips before being formed and finally brazed at an elevated temperature. After a period of natural aging, the final product is operated at two different temperatures depending on the application: about 95 °C for radiators, and peaks up to about 250 °C for charge-air-coolers. For an Al-Mg-Si-Cu alloy type core material, this process translates into solution heat treatment, natural aging and aging during operation. High-resolution imaging with aberration corrected high angle annular dark field scanning transmission electron microscopy (HAADF-STEM) revealed the presence of a complex mix of precipitates after 58 days at 95 °C, including a never-before-reported phase which structurally is a mix between Al-Cu and Al-Mg-Si type precipitates. The stability of this phase is investigated with density functional theory (DFT). Q' is the main phase observed after 5 h at 250 °C, with most precipitates incorporating a certain type of stacking fault.

1. Introduction

Heat exchangers are manufactured by joining a lower melting point alloy, usually a binary Al-Si, with a core material which can be an Al-Mg-Si-Cu alloy, during a brazing process usually at temperatures up to 600 °C. When in operation the heat exchangers reach elevated temperatures which, depending on the application, are up to 95 °C for radiators, and 250 °C for charge-air-coolers. These thermal cycles are interesting because during brazing the core material is subjected to a solution heat treatment (SHT) above the solvus line which is above ~500 °C for Al-Mg-Si(-Cu) alloys, while during operation the material is experiencing an artificial aging (AA). Common AA temperatures for conventional Al-Mg-Si(-Cu) alloys are between 150 °C and 200 °C, which means that heat exchangers operate at lower (95 °C) and higher (250 °C) values. Based on these observations the focus of the present work is to investigate the microstructure development of the core material during the operation of heat exchangers. In general, for Al-Mg-Si(-Cu) alloys, a super-saturated solid solution (SSSS) is formed during the rapid cooling from SHT. Fast diffusion of solute elements using the excess vacancies leads to the formation of atomic clusters that evolve into high number densities of nano-sized metastable precipitates in the Al matrix during the subsequent AA, giving strength and other properties to the material. Therefore, hardening precipitates is the main microstructure constituent in such alloys, and they will be the subject of the investigation in the present work. For conventional Al-Mg-Si(-Cu) alloys extensive research has been performed to relate precipitate parameters (number densities, sizes, types) to both processing and final properties [1,2]. For the Al-Mg-Si system the precipitation sequence was found as:

SSSS - > atomic clusters - > β″ [3] - > β' [4], U1 [5], U2 [6], B' [7] - > β, Si (stable),

where the U1, U2 and B′ phases are also called Type A, Type B and Type C respectively [8].

With Cu additions new phases form, and the main hardening phase in the Cu-free system, β″, is suppressed. The precipitation sequence becomes:

SSSS - > atomic clusters - > β″, L, S, C, β'_{Cu}, Q' - > Q (stable) [9–13].

All metastable precipitates have one main coherency direction with the Al matrix, along ⟨100⟩Al. Consequently, they grow as needles/rods/laths along these directions. Although the metastable phases have different space group symmetries and compositions, they all incorporate the so-called 'Si network' defined by a near hexagonal projection with a ~0.4 nm of the Si atomic columns as viewed along the needle direction [6,9,10,12]. In the case of the monoclinic β″ phase this network is fragmented, due to its high coherency with the Al matrix [14]. True atomic resolution imaging of these precipitates is difficult to obtain with traditional techniques such as high-resolution transmission

* Corresponding author at: SINTEF Industry, Materials and Nanotechnology Sector, Hogskoleringen 5, Trondheim, Norway.
E-mail address: calin.d.marioara@sintef.no (C.D. Marioara).

https://doi.org/10.1016/j.matchar.2019.01.035
Received 10 October 2018; Received in revised form 2 January 2019; Accepted 30 January 2019
Available online 31 January 2019

electron microscopy (HRTEM). However, major progress has been made with the development of spherical aberration (Cs) probe corrected HAADF-STEM technique. The images formed in this way are the result of an incoherent electron scattering process and are therefore more directly interpretable. They are generally unaffected by small changes in the objective lens defocus and specimen thickness, have *Z*-contrast and sub-Ångström spatial resolutions [15–17]. Using this technique, it was discovered that, especially for the Cu-containing Al-Mg-Si alloys, many precipitates have disordered structures with fragments from the metastable phases mentioned above co-existing in one needle [2,9,10,12]. However, although these precipitates lack a unit cell, they still incorporate an undisturbed Si-network in most cases. Another observation is that these fragments consist of stable units unique to the precipitate-types [10]. For example, the Cu local symmetry unit can connect in two different ways, generating the C-phase or the Q' [10–12]. In the case of β″ the basic unit is sometimes called 'the eye' due to the round projected symmetry of the eight atomic columns positioned around the Mg1 sites that constitute unit cell corners [3]. It can connect in three different ways, giving rise to β″ (main occurrence), β''_2 and β''_3 [18]. These findings depict a complex precipitation constellation for the Al-Mg-Si(-Cu) alloys, governed by the alloy's composition and thermo-mechanical treatment. It is also common practice that, once the atomic structure of metastable phases is established based on TEM methods, their stability is investigated by DFT using first principles calculations. This is to ensure the constructed atomic models are correct, and to test for chemical variations in the structure, by probing different possible compositions of certain atomic columns [3]. In this paper we will investigate down to atomic level the hardening metastable precipitates that form in heat exchangers during their operation at 95 °C and 250 °C and compare our findings to precipitate phases described above that have been observed forming during AA at more conventional temperatures and alloys.

2. Material and experimental methods

An alloy with composition (wt%) 0.74Si, 0.27 Mg, 0.29Cu, 0.33Fe, 0.59Mn and 0.14Ti was cast, hot rolled with clad and cold rolled to 0.8 mm thick sheets. As only the core material was studied in the present work, the clad was etched away and the remaining material was measured to approximately 0.4 mm thick plates. It was then subjected to 6 min at 600 °C to simulate brazing, which also acted as SHT. The cooling was done in air until room temperature (RT) was reached. The material was then stored 14 days at RT, which in practice is the usual time between manufacturing and use of the heat exchangers. Two different conditions were made, corresponding to aging for 58 days at 95 °C and 5 h at 250 °C respectively.

TEM specimens were electropolished with a TenuPol-5 machine, using a mixture of 1/3 HNO_3 and 2/3 methanol kept at −25 °C, and a voltage of 20 V. To measure precipitate statistics (number density, average needle cross-section, length and volume fraction), a Jeol JEM-2100 TEM equipped with a LaB_6 filament and operated at 200 kV was used in bright field (BF) mode, following the methodology described in [1]. The instrument was equipped with a Gatan imaging filter (GIF), used for specimen thickness measurement. A double aberration-corrected (image and probe Cs) cold-FEG Jeol ARM-200F operated at 200 kV was used for the HAADF-STEM imaging. The probe size was 0.08 nm, the convergence semi-angle was 28 mrad and the inner and outer collection angles were 35 and 150 mrad, respectively. The inner collection angle is somewhat smaller than what is considered optimal for HAADF-STEM (50 mrad), but our experience is that the lower *Z*-contrast Mg-containing atomic columns are better resolved with this setting. Due to the specific crystallographic orientation of the needle precipitates in the Al-Mg-Si(-Cu) alloy system, all images presented in this work are taken along ⟨001⟩Al directions. Atomic resolution HAADF-STEM images in general have low signal-to-noise ratio and have a grainy appearance. This means that such noise manifests itself at higher spatial frequencies in the fast fourier transform (FFT) of the images than the useful information, which is the position of projected atomic columns of the structure. For this reason, to improve clarity, all the HAADF-STEM images shown in this paper are filtered using a circular bandpass mask applied on the respective FFTs, and an inverse FFT (IFFT) was performed on the masked area suppressing all features with separation shorter than 0.15 nm in the real space. It should be noted that 0.15 nm is close to the minimum projected atomic column separation for precipitates in the Al-Mg-Si(-Cu) system viewed along their needle lengths.

Density functional theory calculations

The formation enthalpies of selected structures were calculated with density functional theory (DFT) using the Vienna ab initio simulation package (VASP) [19,20], applying the projector augmented wave method within the Perdew-Burke-Ernzerhof (PBE) generalized gradient approximation [21]. The plane wave energy cut-off was 400 eV and a Γ-centered 2 × 1 × 9 k-points mesh were used, corresponding to a maximal k-point distances of 0.18 $Å^{-1}$ in each direction. The electronic accuracy for self-consistent loops was set at 10^{-6} eV. The atomic positions were relaxed to a maximum force of 0.001 eV/Å between atoms, using first-order Methfessel-Paxton for smearing of partial occupation with a smearing factor of 0.2. For accurate energies, we conducted a separate calculation using the tetrahedron method with Blöchl correction for the smearing. All the DFT calculations were performed in periodic slabs consisting of 6 × 12 × 1 Al FCC unit cells (288 atoms) with lattice parameter relaxed to a = 4.0399 Å. Hence, we assume full periodicity along the [001]Al "viewing" direction. The formation enthalpies were calculated as

$$\Delta H = E_{Al_{n_1}Mg_{n_2}Si_{n_3}Cu_{n_4}} - (n_1E_{Al} + n_2E_{Mg} + n_3E_{Si} + n_4E_{Cu}), \quad \text{where } \sum_i n_i = 288,$$

$E_{Al_{n_1}Mg_{n_2}Si_{n_3}Cu_{n_4}}$ is the energy of a slab with n_1, n_2, n_3 and n_4 Al, Mg, Si and Cu atoms, respectively. The reference energies was chosen as follows; $E_{Al} = E_{Al_{288}}/288$ is the energy of a bulk Al atom, while E_{Mg}, E_{Si} and E_{Cu} correspond to the energy per atom for a row along the [001]Al direction of solute Mg, Si and Cu atoms, respectively. Hence $E_X = E_{Al_{287}X} - 287E_{Al}$, with X = Al, Mg, Si, Cu.

3. Results and discussion

BF images from the two analyzed conditions are presented in Fig. 1 and show a significant difference in precipitate parameters, which is reflected in the large magnification difference used to visualize the precipitates. It can also be observed that in the condition aged at 250 °C (Fig. 1b) needle precipitates are nucleated both in the matrix and on dispersoids, due to slow cooling from SHT and high aging temperature. The measured precipitate parameters, listed in Table 1, show a large number density of short precipitates in the condition aged at 95 °C, while in the condition aged at 250 °C the number density is greatly reduced. In addition, the aspect ratio (length versus width) of precipitates is much higher in the latter. For this condition Table 1 also includes parameters of the precipitates nucleated on dispersoids. The number density of these precipitates was calculated by counting the number density of dispersoids and assume, based on careful analysis of the images, that on average one needle precipitate is nucleated on one dispersoid. It is interesting to notice that precipitates nucleated on dispersoids are on average shorter and thicker than the ones nucleated in the matrix, as can qualitatively be observed in Fig. 1b. While aging at 250 °C produces needle precipitates which are clearly observed in all < 100 > Al directions, most precipitates formed at 95 °C are only visible in cross-section. This can be understood by the small needle size formed at 95 °C, in particular the cross-section area. Consequently, these needles give a low contrast when viewed perpendicular. The sections below present and discuss the precipitate-types observed by HAADF-STEM in these two investigated conditions.

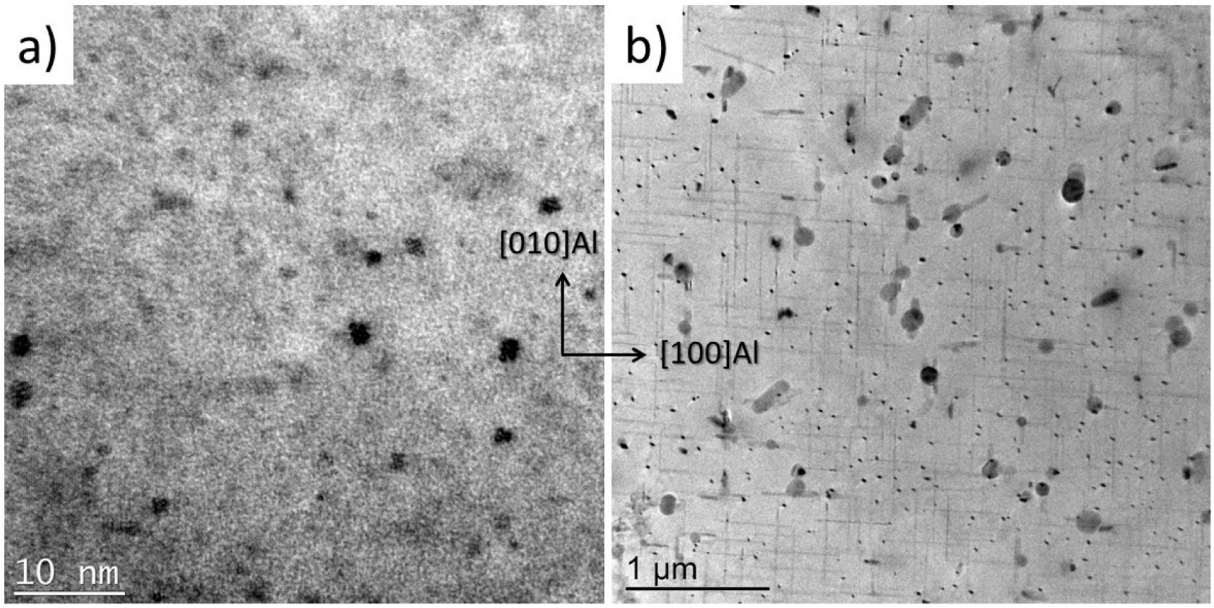

Fig. 1. Bright field TEM images of a) condition with aging 58 days at 95 °C and b) condition with aging 5 h at 250 °C. A large difference in precipitate density and size is observed between the conditions. In b) nucleation of large needles on dispersoids is also observed.

3.1. Condition with aging for 58 days at 95 °C

Subjecting the material to an extended period of time at a temperature which is below the usual aging temperature range produced a complex and interesting precipitate mix, with three main components when the atomic structure is considered.

The first category is given by precipitates based on the β″ basic unit, or the 'eye', with examples given in Fig. 2. The main characteristics of such precipitates can be summarized as following:

- The eyes can connect in various ways, the standard monoclinic arrangement (Fig. 2a, b) [3,18] being one of them. This has been reported before, as being enhanced by Ge and Li additions to Al-Mg-Si alloys [18]. In Fig. 2d a β''_2 is marked by dashed line, while the dotted lines in Fig. 2c, d mark a new connection of the eyes which we should name β''_4. A common element between these arrangements is that the eyes always connect along the ⟨310⟩Al and ⟨320⟩Al directions. In the standard monoclinic β″ arrangement one unit cell direction is along < 310 > Al, and the other along ⟨320⟩Al forming perfectly coherent interfaces all around the cross-section.
- The eyes can make incomplete, or fractional unit cells, as illustrated in Fig. 2b and the upper left three-eyes β″ precipitate in Fig. 2e.
- Weak Cu incorporation occurs mostly at the Si3/Al sites of β″, which confirms findings of previous works [22,23].
- Single β″ eyes have also been observed, illustrated in the lower part of Fig. 2e. This demonstrates the stability of the eye basic unit, that can exist independently in the Al matrix.

The main characteristic of the second category is the presence of Cu-enriched {200}Al planes, or 'Cu-walls' viewed edge on, in two different instances:

- One Cu-wall forms at the interface of larger needle precipitates. These precipitates are disordered, incorporate β″ eyes and have weak Cu enrichment at their interior. See Fig. 3a, b.
- Cu-walls form alone, nucleated on dislocation lines. Fig. 3c shows two Cu-walls having a common nucleation point, and in Fig. 3d three Cu-walls form at different locations along a dislocation line.

The third category includes a new type of needle precipitate, characterized by a coherent interface of two short Cu-walls, always separated by 6 $d_{200}{}^{Al}$, as seen in Fig. 4. Moreover, Mg, Si and to a lesser extent Cu is present in-between the walls, in a disorderly fashion. Sometimes these elements seem to enrich the FCC Al matrix (Fig. 4a to c), other times they arrange into full or incomplete β″ eyes usually located outside the walls (see Fig. 4d to f). In e) the eyes connect as β''_2. In most cases there is at least one Cu-enriched atomic column in the middle location between the walls.

The presence of Cu-walls with 6 $d_{200}{}^{Al}$ separation in this precipitate type is interesting due to its similarity with the Al-Cu system. The main precipitate types there are large θ″ and θ′ plates with {200}Al habit planes. They are delimited at interface by the same (although much larger) Cu-walls (planes), with 4 $d_{200}{}^{Al}$ separation for θ″ and minimum 6 $d_{200}{}^{Al}$ separation for θ′ [24]. An image containing both θ″ and θ′ plates from an Al - 5 wt% Cu alloy is shown in Fig. 5. The similarity with the θ′ plates from the Al-Cu system indicates the Al-Mg-Si-Cu precipitates in Fig. 4 are a fusion between the Al-Mg-Si and Al-Cu systems. They are composed by a Mg-Si dominated core and delimited by two Cu-walls separated by 6 $d_{200}{}^{Al}$. To understand the role of each part to precipitate stability, DFT calculations were conducted on a 288

Table 1
Measured precipitate (needle) parameters (precipitate volume density, average needle length and cross-section, as well as precipitation volume fraction) for the two investigated conditions. The first two rows show the parameters of precipitates nucleated in the matrix (bulk), while the condition marked with the asterisk indicates the parameters of precipitates nucleated on dispersoids for the condition aged at 250 °C.

Condition/parameter	< Density > (μm^{-3})	< Length > (nm)	< Cross section > (nm^2)	< Volume fraction > = D x L x CS (%)
58d at 95 °C	916,180 ± 91,911	4.37 ± 0.10	1.28 ± 0.05	0.51 ± 0.06
5 h at 250 °C	90.29 ± 12.43	550.00 ± 63.83	110.22 ± 7.31	0.55 ± 0.20
5 h at 250 °C*	10.00 ± 1.28	298.27 ± 16.63	605.40 ± 41.23	0.18 ± 0.03

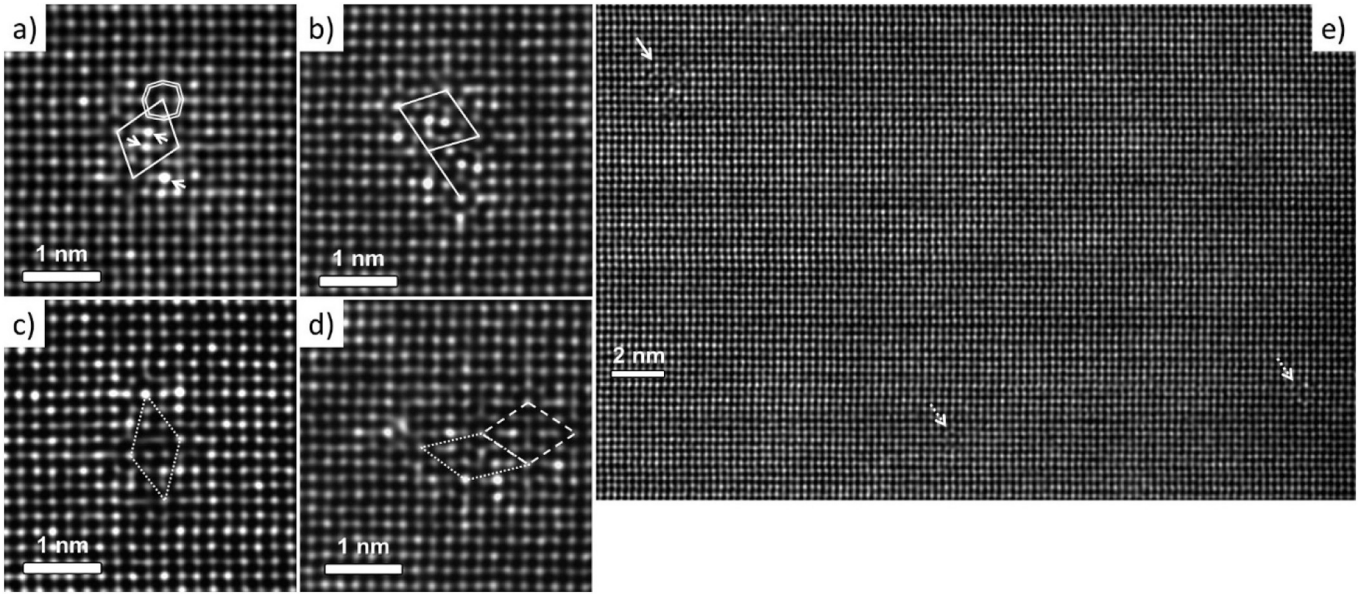

Fig. 2. HAADF-STEM high resolution images from condition aged 58 days at 95 °C show precipitates based on β″ eyes. In a) to d) the eye centers are connected by single lines, with continuous lines marking the normal monoclinic β″, the dashed lines mark the β''_2 and the dotted lines mark the β''_4 eye arrangements. In a) one eye is marked with double lines and Cu enrichment at Si3/Al sites is shown by arrows. In e) the full-line arrow shows an incomplete monoclinic three eye arrangement, and the dotted line arrows mark two single β″ eyes.

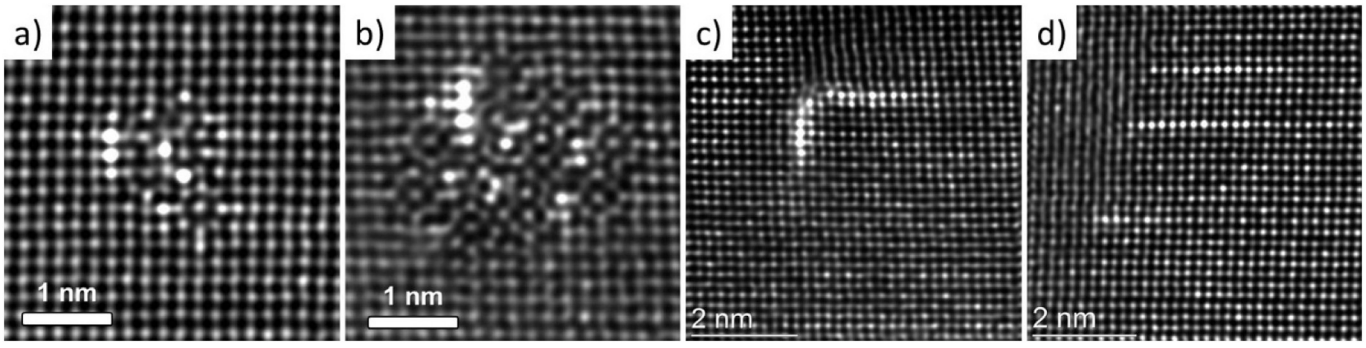

Fig. 3. HAADF-STEM high resolution images from condition aged 58 days at 95 °C show Cu walls forming at interfaces of needle precipitates (a, b) and nucleated alone on dislocations (c, d). The presence of dislocations is revealed by the wavy appearance of the matrix atomic columns, which occurs on middle-top of c) and on the up-left corner in d).

atoms cell in which precipitate configurations were constructed with 4, 6 and 8 $d_{200}{}^{Al}$ Cu-wall separation, and interior consisting of Mg, Si atoms substituting Al on its FCC lattice. For each wall separation, formation enthalpies were calculated for the walls + Mg, Si precipitate, only walls (with Al matrix in-between) and only Mg, Si part configurations (no walls). The results of these calculations are presented graphically in Fig. 6. It should be noted that, due to the different solute concentrations for each wall separation, only configurations with same wall separation can be directly compared.

Comparisons between configurations with different wall separations can be expressed as differences in trends. With these considerations, it is observed that walls + Mg, Si configurations are most stable for each wall separation. Removing the walls results in loss of stability, being most pronounced at 4 $d_{200}{}^{Al}$ wall separation, and least pronounced at 8 $d_{200}{}^{Al}$ wall separation. On the contrary, removing the Mg-Si part and leaving only the walls and Al results in largest stability loss for 8 $d_{200}{}^{Al}$ wall separation, and lowest for the 4 $d_{200}{}^{Al}$ wall separation configurations. In other words, the stabilizing effect of the Cu-walls is greatest at short wall separation, while the stabilizing effect of the Mg-Si ordering is greatest at large wall separations. Although these calculations do not answer the question why the precipitates in Fig. 4 have always 6 $d_{200}{}^{Al}$ wall separation, it is believed this is an energetic compromise between these two opposite effects.

3.2. Condition with aging for 5 h at 250 °C

As Fig. 1 and Table 1 indicate, the precipitate microstructure in this condition is much coarser than that formed during aging at 95 °C. HAADF-STEM images indicated that all investigated precipitates were of Q/Q' type [9,13], regardless if they were bulk precipitates, or nucleated on dispersoids. An example of dispersoid-nucleated precipitate is presented in Fig. 7, while Fig. 8 gives two examples of bulk-nucleated precipitates. These images show that, although all precipitates are Q/Q' in nature which easily can be recognized by the typical hexagonal distribution of the Cu-containing atomic columns, the particles contain large disordered areas, stacking faults and consequently more irregular interfaces with the Al matrix. One type of stacking fault was observed in almost every bulk precipitate, indicated by arrows in Fig. 8. In order to elucidate its atomic arrangement, an atomic overlay was conducted on a more coherent precipitate, shown in Fig. 9. The overlay is based on the known crystal structure of Q/Q' phase, *Z*-contrast information in the HAADF-STEM image, and construction rules of precipitates in the 2xxx and 6xxx Al alloy systems from [14]. According to these rules, every Al atom has 12 near neighbors, every Mg atom has 15 and every Si has 9.

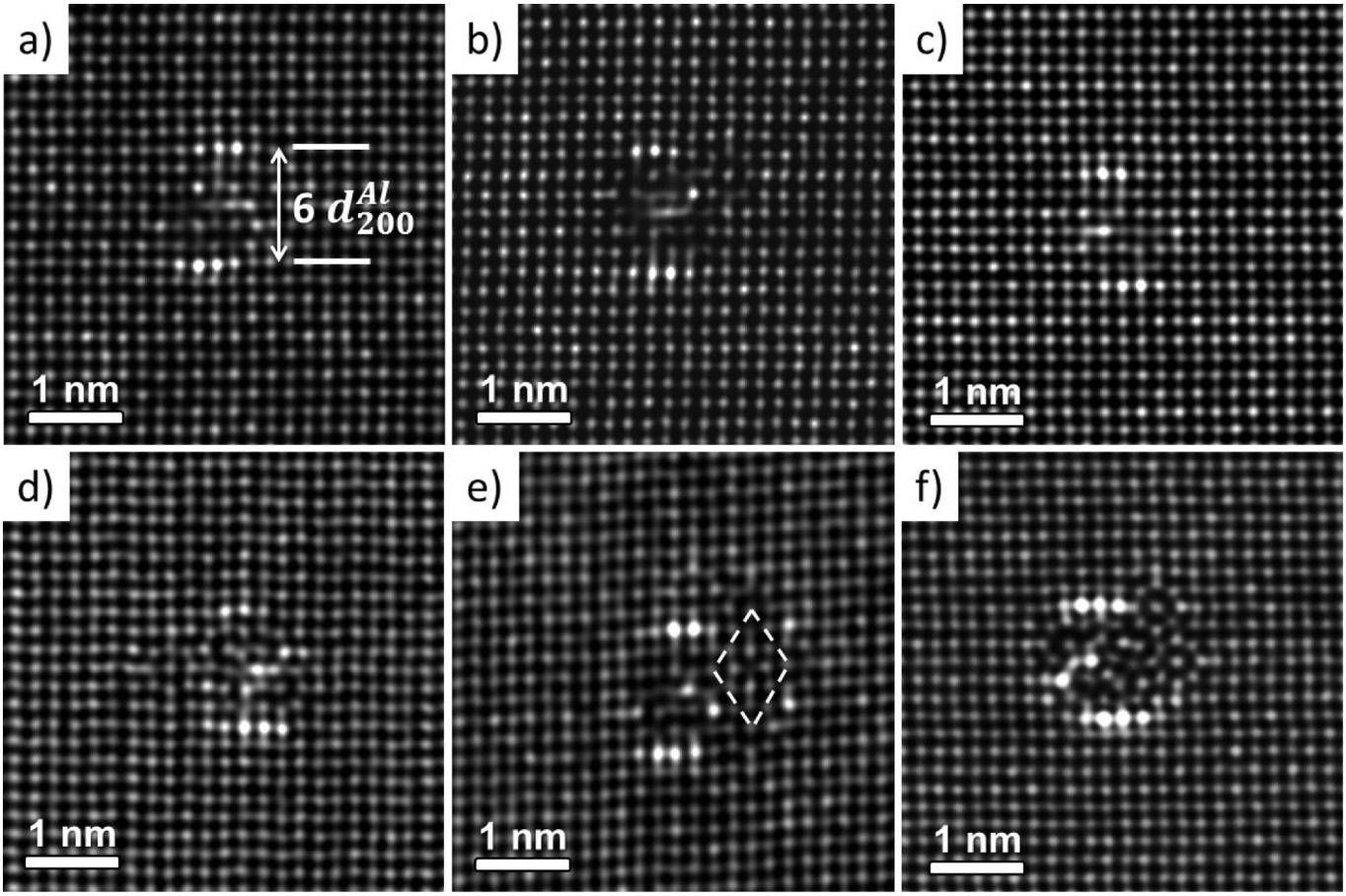

Fig. 4. HAADF-STEM high resolution images from condition aged 58 days at 95 °C show a new precipitate-type with Mg, Si, Cu solute delimited by two Cu-walls always separated by 6 $d_{200}{}^{Al}$. The dashed line in e) connects centers of β″ eyes stacked as β''_2.

It means that in the overlay every Al atom is surrounded by 4 atoms of opposite height, every Mg by 5 and every Si by 3 (making it a triangular site). It is interesting to notice that Cu in the Q' unit cell is a triangular site (has 9 near neighbors like Si), but a few Cu atoms at the incoherent interface (on the right side of the particle) and all the Cu in the stacking fault have 12 near neighbors, as Al. A few observations can be made from Fig. 9:

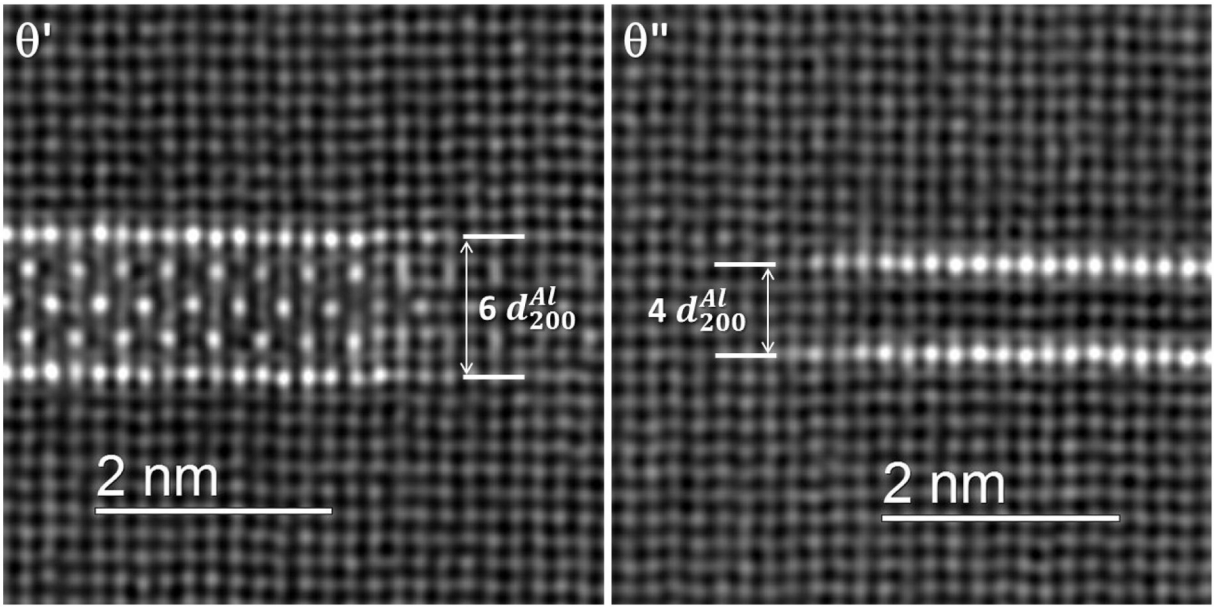

Fig. 5. HAADF-STEM high resolution images from an Al - 5 wt% Cu alloy show a θ′ plate with Cu-walls separated by 6 $d_{200}{}^{Al}$, and a θ″ plate with Cu-walls separated by 4 $d_{200}{}^{Al}$.

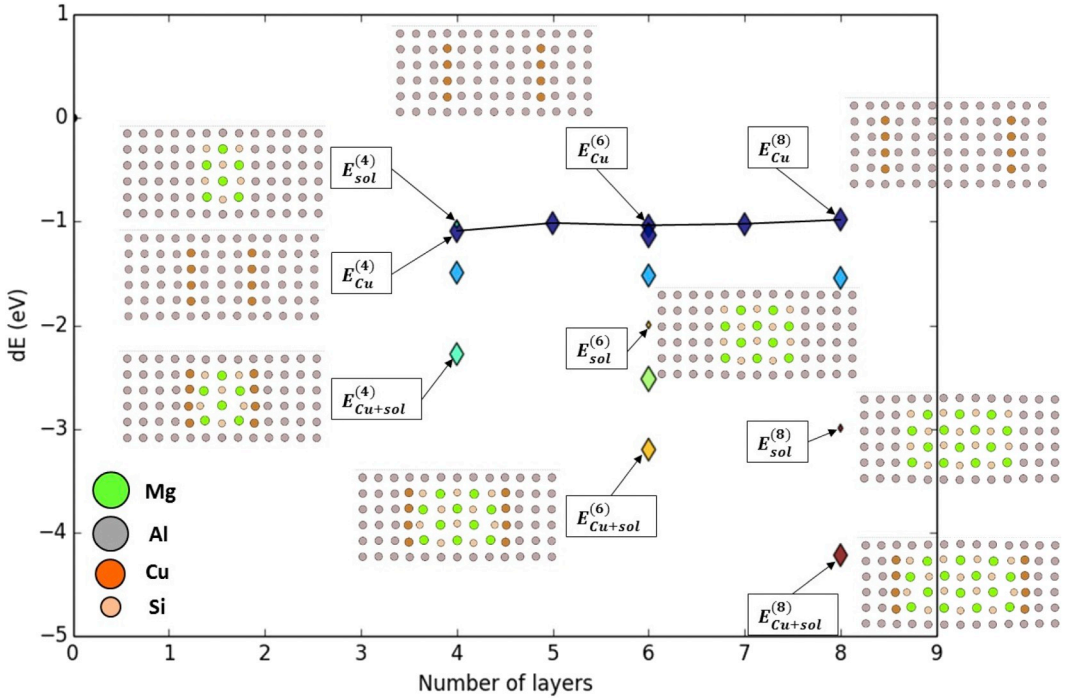

Fig. 6. Formation enthalpies of different precipitate configurations calculated with DFT. The atom configurations are indicated with arrows for some of the cases. Large diamonds refer to configurations with Cu walls and the colour of the diamonds to the number of Mg + Si atoms; dark blue: 0, light blue: 8, cyan: 12, green: 15, orange: 20, dark red: 28. (For interpretation of the references to colour in this figure legend, the reader is referred to the web version of this article.)

- The two interfaces along < 510 > Al are fully coherent with the Al matrix and contain a chain of alternating Mg and Si atomic columns. The interfaces have opposite atomic heights.
- The stacking fault is created by a shift of two rows of Q' unit cells along one of their edges. Also, there is a switch between Al and Mg positions in the alternating Al-Mg-Al-Mg-Al-Mg atomic column configuration around the corner Si for the unit cell corners facing the stacking fault. The Q' unit cells have opposite heights across the stacking fault.
- The projected hexagonal Si network has a continuous, undisturbed presence across the entire precipitate, including the stacking fault. This may indicate the precipitate has a common nucleation source, and the stacking fault is not the result of joining two parts separately nucleated.

It should be noted that formation of Q' phase at temperatures above 200 °C is common in Cu-containing Al-Mg-Si alloys [2,9]. Usually Q' is reported as lath-shaped, with main coherency along < 510 > Al in the cross-section plane. However, the present work shows the large degree of disorder this phase can contain, which also affects its connection to the Al matrix. Further studies are needed to understand the relationship between heat treatment, precipitate size, coherency with the Al matrix and material hardness.

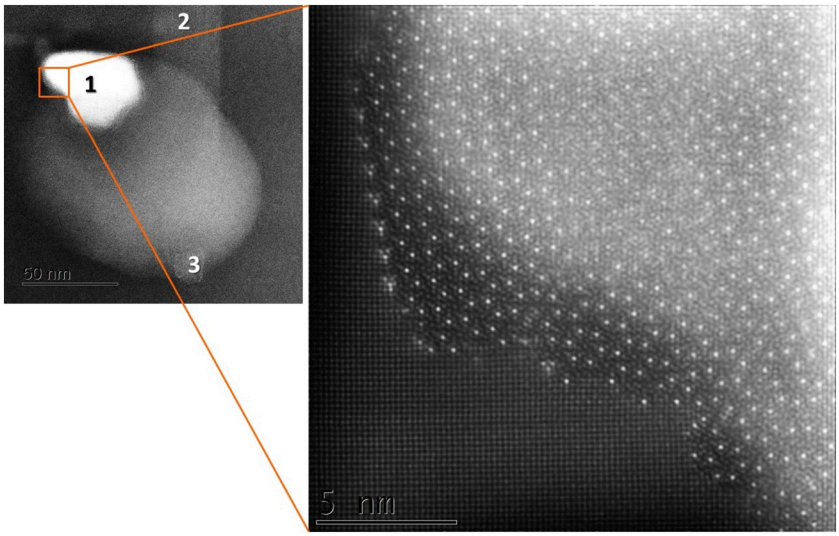

Fig. 7. HAADF-STEM images of three needle precipitates nucleated on a dispersoid. Numbers 1 and 3 are viewed in cross-section, and number 2 is viewed perpendicular. The enlarged part shows a Q/Q' atomic structure.

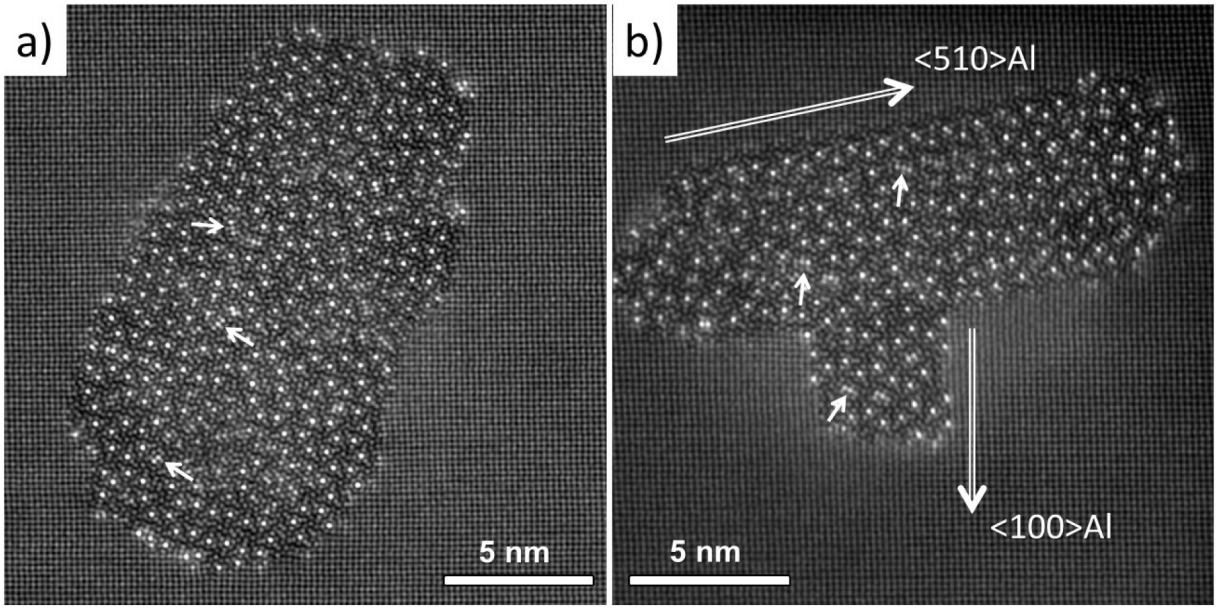

Fig. 8. HAADF-STEM images of two precipitates in the bulk. The precipitate in a) has an irregular interface, and the one in b) has two coherent interfaces, along < 510 > Al and ⟨100⟩Al. Both precipitates contain similarly looking stacking faults, some of which are indicated by short full-line arrows.

4. Conclusions

A complex mix of precipitate-types are present after 58 days exposure at 95 °C. They can be classified into four main categories:

1) Collection of β″ eyes forming full, or fractional β″ unit cells. Single β″ eyes have also been observed, and can be included in this category. Weak Cu enrichment of Si3/Al sites was common in these small precipitates.
2) Larger, disordered precipitates containing β″ eyes, Cu enrichment and single, short Cu walls. A Cu wall is basically a Cu-containing {200}Al plane. Cu walls are common in the interfaces of θ″ and θ′ plates from the Al-Cu system.
3) Single Cu walls nucleated on dislocation lines.
4) A unique precipitate-type with interfaces consisting of two short Cu walls separated by 6 $d_{200}{}^{Al}$. Due to *Z*-contrast variations of atomic columns, Mg and Si columns are assumed in-between the walls. This is supported by the occasional presence of full, or partial β″ eyes in-between the walls, and outside it. Low Cu presence is also observed at the interior. As θ′ plates can have interfaces of Cu walls separated

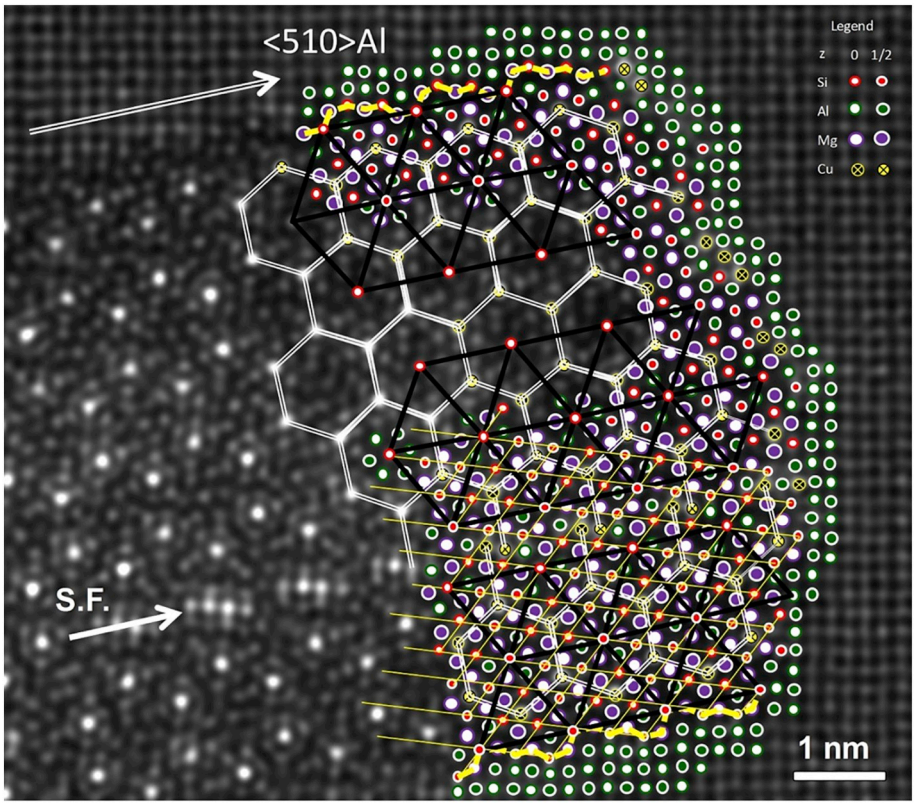

Fig. 9. Atomic overlay of a Q' precipitate imaged in HAADF-STEM, with two coherent interfaces along < 510 > Al (indicated by the dashed thick yellow lines), and a stacking fault (S.F.) line. Cu atomic columns are connected by white double lines, Q' unit cell corners are connected by black lines, and part of the Si network (Si atomic columns) are connected by thin yellow lines. (For interpretation of the references to colour in this figure legend, the reader is referred to the web version of this article.)

by 6 d_{200}^{Al}, the observed precipitate-type may be described as a hybrid between Al-Mg-Si and Al-Cu alloy systems.

Q, or Q' type precipitates were observed nucleated in the bulk and on dispersoids after 5 h aging at 250 °C. They contained high numbers of defects and stacking faults, and a high fraction of them had irregular (less coherent) interfaces. The only fully coherent interfaces grow along the < 510 > Al directions. A common stacking fault is found to preserve the Si-network of the host precipitate. Full atomic models are given for the < 510 > Al coherent interface and for the stacking fault.

Acknowledgements

This work is part of the AMPERE project (247783), a Knowledge-building Project for Industry, co-financed by The Research Council of Norway (RCN) and the industrial partners Norsk Hydro, Sapa, Gränges, Neuman Aluminium Raufoss (Raufoss Technology) and Nexans. RCN and the industrial partners are gratefully acknowledged for their financial support. The TEM analysis was carried out using the NORTEM infrastructure (NFR 197405) at the TEM Gemini Centre Trondheim, Norway. The DFT calculations were performed on resources provided by UNINETT Sigma2 - the National Infrastructure for High Performance Computing and Data Storage in Norway (project nn9128k).

The raw/processed data required to reproduce these findings cannot be shared at this time due to technical or time limitations.

References

[1] C.D. Marioara, S.J. Andersen, H.W. Zandbergen, R. Holmestad, The Influence of alloy composition on precipitates of the Al-Mg-Si system, Metall. Mater. Trans. A 36A (2005) 691–702, https://doi.org/10.1007/s11661-005-0185-1 (ISSN: 1073-5623).

[2] C.D. Marioara, S.J. Andersen, J. Røyset, O. Reisø, S. Gulbrandsen-Dahl, T.E. Nicolaisen, I.E. Opheim, J.F. Helgaker, R. Holmestad, Improving thermal stability in Cu-containing Al-Mg-Si alloys by precipitate optimization, Metall. Mater. Trans. A 45A (2014) 2938–2949, https://doi.org/10.1007/s11661-014-2250-0 (ISSN: 1073–5623).

[3] H.S. Hasting, A.G. Frøseth, S.J. Andersen, R. Vissers, J.C. Walmsley, C.D. Marioara, F. Danoix, W. Lefebvre, R. Holmestad, Composition of β″ precipitates in Al-Mg-Si alloys by atom probe tomography and first principles calculations, J. Appl. Physiol. 106 (12) (2009) 123527, , https://doi.org/10.1063/1.3269714 (ISSN 0021–8979).

[4] R. Vissers, M.A. van Huis, J. Jansen, H.W. Zandbergen, C.D. Marioara, S.J. Andersen, The crystal structure of the β′ phase in Al-Mg-Si alloys, Acta Mater. 55 (2007) 3815–3823, https://doi.org/10.1016/j.actamat.2007.02.032 (ISSN 1359–6454).

[5] S.J. Andersen, C.D. Marioara, R. Vissers, A. Frøseth, H.W. Zandbergen, The structural relation between precipitates in Al-Mg-Si alloys and diamond silicon, with emphasis on the trigonal phase U1-MgAl2Si2, Mater. Sci. Eng. A 444 (2007) 157–169, https://doi.org/10.1016/j.msea.2006.08.084 (ISSN 0921–5093).

[6] S.J. Andersen, C.D. Marioara, A. Frøseth, R. Vissers, H.W. Zandbergen, Crystal structure of the orthorhombic U2-Al4Mg4Si4 precipitate in the Al-Mg-Si alloy system and its relation to the β′ and β″ phases, Mater. Sci. Eng. A 390 (2005) 127–138, https://doi.org/10.1016/j.msea.2004.09.019 (ISSN 0921–5093).

[7] R. Vissers, C.D. Marioara, S.J. Andersen, R. Holmestad, Crystal structure determination of the B' phase in Al-Mg-Si alloys by combining quantitative electron diffraction and ab-initio calculations, Aluminium Alloys (Proceedings of ICAA11, 22–26 September 2008, Aachen, Germany), 2 (2008) 978-3-527-32367-8, pp. 1263–1269.

[8] K. Matsuda, Y. Sakaguchi, Y. Miyata, Y. Uetani, T. Sato, A. Kamio, S. Ikeno, Precipitation sequence of various kinds of metastable phases in Al −1.0 mass% Mg_2Si – 0.4 mass % Si alloy, J. Mater. Sci. 35 (2000) 179–189, https://doi.org/10.1023/A:1004769305736.

[9] C.D. Marioara, S.J. Andersen, T.N. Stene, H. Hasting, J. Walmsley, A.T.J. Van Helvoort, R. Holmestad, The effect of Cu on precipitation in Al-Mg-Si alloys, Philos. Mag. 87 (2007) 3385–3413, https://doi.org/10.1080/14786430701287377 (ISSN 1478–6435).

[10] T. Saito, Eva A. Mørtsell, S. Wenner, Calin D. Marioara, Sigmund J. Andersen, J. Friis, K. Matsuda, R. Holmestad, Atomic structures of precipitates in Al-Mg-Si alloys with small additions of elements, Adv. Eng. Mater. (2018), https://doi.org/10.1002/adem.201800125.

[11] M. Torsæter, F.J.H. Ehlers, C.D. Marioara, S.J. Andersen, R. Holmestad, Applying precipitate-host lattice coherency for compositional determination of precipitates in Al-Mg-Si-Cu alloys, Philos. Mag. 92 (31) (2012) 3833–3856, https://doi.org/10.1080/14786435.2012.693214 (ISSN: 1478–6443).

[12] T. Saito, C.D. Marioara, S.J. Andersen, W. Lefebvre, R. Holmestad, Aberration-corrected HAADF-STEM investigations of precipitate structures in Al–Mg–Si alloys with low Cu additions, Philosophical Magazine, 2014, pp. 1478–6443, , https://doi.org/10.1080/14786435.2013.857051 (vol. 94, issue 5, 520–531 ISSN 1478–6435 (Print)).

[13] S. Wenner, L. Jones, C.D. Marioara, R. Holmestad, Atomic-Resolution Chemical Mapping of Ordered Precipitates in Al Alloys Using Energy-Dispersive X-ray spectroscopy, 96 Micron, 2017, pp. 103–111, https://doi.org/10.1016/j.micron.2017.02.007 (ISSN: 0968–4328).

[14] S.J. Andersen, C.D. Marioara, J. Friis, R. Bjørge, Q. Du, I.G. Ringdalen, S. Wenner, E.A. Mørtsell, T. Saito, J. Røyset, O. Reiso, Directionality and column arrangement principles of precipitates in Al-Mg-Si-(Cu) and Al-Mg-Cu linked to line defect in Al, Materials Research Forum, vol. 877, 2016, pp. 461–470, , https://doi.org/10.4028/www.scientific.net/MSF.877.461 (ISSN 1662–9752).

[15] P.D. Nellist, S.J. Pennycook, The principles and interpretation of annular dark-field Z-contrast imaging, Adv. Imaging Electron Phys. 113 (2000) 147–203, https://doi.org/10.1016/S1076-5670(00)80013-0.

[16] T. Yamazaki, M. Kawasaki, K. Watanabe, I. Hashimoto, M. Shiojiri, Effect of small crystal tilt on atomic-resolution high-angle annular dark field STEM imaging, Ultramicroscopy 92 (2002) 181–189, https://doi.org/10.1016/S0304-3991(02)00131-6.

[17] H. Rose, Theoretical aspects of image formation in the aberration-corrected electron microscope, Ultramicroscopy 110 (2010) 488–499, https://doi.org/10.1016/j.ultramic.2009.10.003.

[18] E.A. Mortsell, S.J. Andersen, J. Friis, C.D. Marioara, R. Holmestad, Atomistic details of precipitates in lean Al-Mg-Si alloys with trace additions of Ag and Ge studied by HAADF-STEM and DFT, Philosophical Magazine, 97(11) 2017, pp. 851–866, , https://doi.org/10.1080/14786435.2017.1281461 (part A, ISSN: 1478–6435, eISSN: 1478–6443).

[19] G. Kresse, J. Furthmuller, Efficiency of ab initio total energy calculations for metals and semiconductors using a plane wave basis set, Comput. Mater. Sci. 6 (1996) 15–50, https://doi.org/10.1016/0927-0256(96)00008-0.

[20] G. Kresse, J. Hafner, Ab initio molecular dynamics for liquid metals, Phys. Rev. B 47 (1) (1993) 558–561, https://doi.org/10.1103/PhysRevB.47.558.

[21] J.P. Perdew, K. Burke, M. Ernzerhof, Generalized gradient approximation made simple, Phys. Rev. Lett. 77 (18) (1996) 3865–3868, https://doi.org/10.1103/PhysRevLett.77.3865.

[22] K. Li, A. Béché, M. Song, G. Sha, X. Lu, K. Zhang, Y. Du, S.P. Ringer, D. Schryvers, Atomistic structure of Cu-containing β″ precipitates in an Al-Mg-Si-Cu alloy, Scr. Mater. 75 (2014) 86–89, https://doi.org/10.1016/j.scriptamat.2013.11.030.

[23] T. Saito, F.J.H. Ehlers, W. Lefebvre, D.H. Maldonado, R. Bjørge, C.D. Marioara, S.J. Andersen, E.A. Mørtsell, R. Holmestad, Cu atoms suppress misfit dislocations at the β″/Al interface in Al-Mg-Si alloys, Scr. Mater. 110 (2016) 6–9, https://doi.org/10.1016/j.scriptamat.2015.07.033 (ISSN 1359–6462).

[24] L. Bourgeois, C. Dwyer, M. Weyland, J.F. Nie, B.C. Muddle, Structure and energetics of the coherent interface between the θ' precipitate phase and aluminium in Al-Cu, Scr. Mater. 59 (2011) 7043–7050, https://doi.org/10.1016/j.actamat.2011.07.059.